Kinetics of Photocatalytic Decomposition of Methylene Blue

Chun-Hsing Wu and Jia-Ming Chern*

Department of Chemical Engineering, Tatung University, 40 Chungshan North Road, 3rd Section, Taipei 10452, Taiwan

To treat dyeing and finishing industrial wastewater effluents by an advanced oxidation process, the decomposition kinetics of methylene blue by nanofine sol TiO_2/UV was systematically studied in two batch slurry reactors. The factors of study include agitation speed, recirculation flow rate, initial dissolved oxygen concentration, initial methylene blue concentration, reaction temperature, TiO_2 dosage, and UV light intensity. By using the network reduction technique, the general rate equation has been developed from considering the reaction mechanism. The rate equation uses a systematic reaction network reduction technique to avoid the need of more restrictive assumptions commonly used, such as a rate-determining step or equilibrium steps. The resulting rate equation is applicable to a wider range of reaction conditions. After applying the resulting rate equation to predict the transient concentrations of other dye compounds, we expect it can be applied for the kinetics of photodecomposition of other organic compounds.

Introduction

Manufacturing processes of dyeing and finishing industries always use a lot of dyestuff, but only part of the dyestuff is really utilized. The rest of the dye compounds dissolve in wastewater effluent entering water bodies such as rivers and lakes. During a chemical or biological reaction pathway, these dye compounds not only deplete the dissolved oxygen in water bodies but also release some toxic compounds to endanger aquatic life. To protect the aquatic environment, many methods such as adsorption, electrocoagulation, ultrasonic decomposition, advanced chemical oxidation, nanofiltration, and chemical coagulation followed by sedimentation were used to remove dyes from wastewater.[1−7] Specifically, advanced oxidation processes (AOPs) involving hydroxyl radical, a very powerful chemical oxidant that can destroy a wide range of tough organic contaminants, are introduced to treat textile dyes effluents.[8−11] Because of the advantages of photocatalytic decomposition of dye wastewaters using TiO_2 particles or films, advanced oxidation by TiO_2/UV has been gaining industrial and academic attention.[12−16]

Most studies on organic compound decomposition with TiO_2/UV investigated some factors that might influence the degradation rate of the organic compounds and proposed some kinetic models to explain their results. Ollis[17] proposed that the rate of reaction was proportional to the coverage of the surface by an adsorbed intermediate. He further assumed the coverage was given by the Langmuir isotherm; the reaction rate he obtained was, thus, of the Langmuir−Hinshelwood rate form. With a plot of reciprocal initial rate vs reciprocal initial concentration, the rate constant and the equilibrium constant were obtained. Ollis used the Langmuir−Hinshelwood rate equation to obtain the rate parameters of dichloromethane and other halogenated hydrocarbon contaminants in water. Since the model and the method Ollis used are easy to follow, many studies just adopt the same model and method to explain their experimental results without considering detailed reaction mechanism. Sivalingam et al.[18] assumed that the disappearance of dye was caused by both direct hole attack and hydroxyl radical attack. After rearranging the decomposition rate equation and omitting the quadratic term, they found the dye decomposition rate was also of the Langmuir−Hinshelwood form. There are some other rate equations, for example, power-law reaction rate, employed for kinetic data analysis. According to their experimental results, Xu et al.[19] proposed that the photodegradation of methylene blue obeyed the first-order reaction law and the rate constant was obtained from the regression of their experimental data.

Some possible photocatalytic reaction mechanisms were proposed, but no explicit rate equations were derived based on the proposed reaction mechanisms. Because the proposed photocatalytic reaction mechanisms are too complicated to be analyzed by the Langmuir−Hinshelwood rate laws, power-law type rate equations were usually used for data analysis. Although the power-law type rate equations can be easily used to correlate kinetic data, these rate equations are empirical in nature and, therefore, cannot be confidently used for reactor design and scale-up. To facilitate obtaining explicit rate equations for complicated reaction networks, Helfferich[20] proposed a systematic approach to elucidation of homogeneous multistep reaction networks; the rate equations for specific reaction networks are recovered by simple substitutions, cancellations, and collection of terms. Chern and Helfferich[21] used the technique of network reduction to obtain the general equations for rates and yield ratios of homogeneous reactions with an arbitrary number of steps and location of nodes and coreactant entries. Chern[22] extended the previous approach to catalytic reactions involving cyclic reaction networks. Chen and Chern[23] further extended the same approach to derive the general reaction rate and rate ratio equations used in catalytic reactions involving multipathway networks. With these tools at hand, the rate equations of complicated networks such as photocatalytic reactions can be more easily derived. This study, therefore, aims at applying the general rate equation approach to study the kinetics of photocatalytic decomposition of a model dye, methylene blue (MB). The general rate equations[22,23] will be directly used to formulate the MB decomposition kinetics. Readers who are interested in the network reduction technique and generate rate approach should refer to Helfferich's book.[24]

* Corresponding author: Tel.: +886-2-27002737 ext. 23. Fax: +886-2-27079528. E-mail: jmchern@ttu.edu.tw.

10.1021/ie0602759 CCC: $33.50
Published on Web 08/10/2006

Unlike most other studies focusing on the dye concentration effect only, this study attempts to experimentally study the effects of many operating factors including agitation speed, recirculation flow rate, initial dissolved oxygen (DO) concentration, initial MB concentration, reaction temperature, TiO_2 dosage, and UV light intensity.

Mechanism and Rate Equation

According to most literature, when aqueous solution was irradiated in the presence of TiO_2 photocatalyst, the adsorbed water molecules reacted with the holes in the valence band to form hydroxyl radicals and release hydrogen ions. Furthermore, the dye molecules might be decomposed to form organic acids as the intermediate products. But in our experiments, the methylene blue solutions were premixed with the TiO_2 suspensions before the UV light was turned on to excite the TiO_2 particles. Therefore, we believe that the adsorption of methylene blue onto the TiO_2 particle surface should be the first step in the reaction mechanism. The methylene blue-occupied TiO_2 particles were then excited to generate hydroxyl radical and superoxide radical that both decomposed the adsorbed methylene blue. Therefore, the reaction steps of methylene blue decomposition can be compiled as follows:[25−27]

$$TiO_2 + \text{dye} \leftrightarrow TiO_2\text{−dye} \quad (1)$$

$$TiO_2\text{−dye} + h\nu(\lambda < 390\ \text{nm}) \leftrightarrow TiO_2(e^-,h^+)\text{−dye} \quad (2)$$

$$TiO_2(h^+) + H_2O_{(ads)} \rightarrow TiO_2(OH_{(ads)}\bullet) + H^+ \quad (3)$$

$$TiO_2(h^+) + OH^-_{(ads)} \rightarrow TiO_2(OH_{(ads)}\bullet) \quad (4)$$

$$TiO_2(e^-) + O_{2(ads)} \rightarrow TiO_2(O^-_{2(ads)}\bullet) \quad (5)$$

$$OH_{(ads)}\bullet + \text{dye} \rightarrow \text{intermediate products} \rightarrow \text{degradation products} \quad (6)$$

$$O^-_{2(ads)}\bullet + \text{dye} \rightarrow \text{intermediate products} \rightarrow \text{degradation products} \quad (7)$$

Equation 1 represents the reversible adsorption step of the dye molecules onto the TiO_2 surface. Equations 2−5 constitute the reaction network of the OH free radical and superoxide free radical formation. The OH free radical and the superoxide free radical will attack the preadsorbed dye compound as shown in eqs 6 and 7, respectively. From the above reaction mechanism, the reaction network is shown in Figure 1a. Figure 1b uses the X notations to represent all the surface species: $X_0 = TiO_2$ (the free site), $X_1 = TiO_2 + \text{dye}$ (the adsorbed dye), $X_2 = TiO_2^* + \text{dye}$ (the excited dye-occupied site), $X_3 = TiO_2\text{−}OH\bullet + \text{dye}$ (the adsorbed hydroxyl radical), and $X_3' = TiO_2\text{−}O_2\bullet + \text{dye}$ (the adsorbed superoxide radical).

The concentrations of the five surface species in the proposed reaction network can be solved from five algebraic equations, four from the pseudo steady-state hypothesis and one from the total site balance. Theoretically, once the concentrations of the five surface species are solved, the dye decomposition rate can be expressed as $-r_{dye} = k_{01}[\text{dye}][X_0] - k_{10}[X_1]$. Using this approach, the general rate equation of dye decomposition can be obtained without assuming any rate-determining or equilibrium step(s). However, solving the five algebraic equations simultaneously is very time-consuming and tedious; this study will directly use the general rate equation for cyclic reaction networks to formulate the rate equation of dye decomposition.[23]

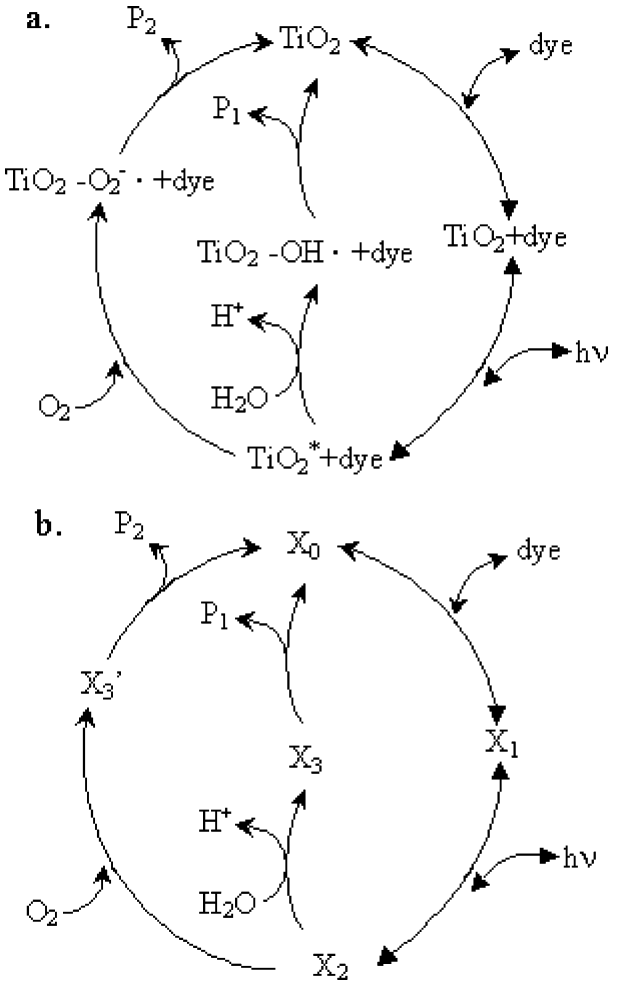

Figure 1. (a) Proposed organic compound decomposition pathway by photocatalytic reaction system. (b) Denotes the proposed photocatalytic reaction network by P and X notations for analysis.

The cyclic reaction network contains one small independent cyclic pathway; the multipathway between X_2 and X_4 ($X_4 = X_0$) may contain an arbitrary number of intermediates. The pathway between X_2 and X_4 can be reduced to one pseudosingle step with the replacement of Λ coefficients by the loop coefficients L defined as

$$\begin{cases} L_{24} = \Lambda_{24}^{(1)} + \Lambda_{24}^{(2)} \\ L_{42} = \Lambda_{42}^{(1)} + \Lambda_{42}^{(2)} \end{cases} \quad (8)$$

Here, the superscript in the Λ coefficients is the pathway number. With such loop coefficients, the reaction network can be reduced to a single cycle network and the dye decomposition rate equation can be expressed as follows,

$$-r_{dye} = \frac{\lambda_{01}\lambda_{12}L_{24}[TiO_2]}{D_{00} + D_{11} + D_{22}(1 + C_{23}^{(1)} + C_{23}^{(2)})} \quad (9)$$

where

$$\lambda_{01} = k_{01}[\text{dye}]; \quad \lambda_{10} = k_{10}$$
$$\lambda_{12} = k_{12}[h\nu]; \quad \lambda_{21} = k_{21}$$

$$\lambda_{23} = k_{23}; \quad \lambda'_{23} = k'_{23}[O_2]$$

$$\lambda_{34} = k_{34}; \quad \lambda'_{34} = k'_{34}$$

$$L_{24} = k_{23} + k'_{23}[O_2] \tag{10}$$

$$D_{00} = \lambda_{12}L_{24} + \lambda_{10}L_{24} + \lambda_{10}\lambda_{21}$$

$$D_{11} = \lambda_{01}L_{24} + \lambda_{01}\lambda_{21}$$

$$D_{22} = \lambda_{01}\lambda_{12}$$

$$C_{23}^{(1)} = \frac{k_{23}}{k_{34}}; \quad C_{23}^{(2)} = \frac{k'_{23}[O_2]}{k'_{34}}$$

Without assuming which reaction step is the rate-determining step, the general rate equation of multipathway type networks can be applied systematically to obtain the explicit rate equation.[20−23]

$$-r_{dye} = k_{01}k_{12}L_{24}[h\nu][dye][TiO_2]/$$
$$k_{10}k_{21} + (k_{10} + k_{12}[h\nu] + k_{01}[dye])(k_{23} + k'_{23}[O_2]) +$$
$$k_{01}k_{21}[dye] + \left(1 + \frac{k_{23}}{k_{34}} + \frac{k'_{23}[O_2]}{k'_{34}}\right)k_{01}k_{12}[dye][h\nu] \tag{11}$$

Equation 11 expresses the dye decomposition rate as a function of the UV light intensity, dye concentration, dissolved oxygen concentration, and TiO_2 suspension concentration.

Experimental Section

Materials. Methylene blue (Merck, Germany), a cationic thiazine dye, with dye content above 82% and molecular weight 319.86 g/mol, was directly used without further purification. Figure 2 shows the UV/vis absorbance spectrum of the methylene blue solution. Hombikat XXS 100 (Sachtleben Chemie Gmbh, Germany), the photocatalyst, consists of a liquid, nanofine sol of pure titanium dioxide in water. The photocatalyst slurry possesses density 1.12 g/cm^3 with TiO_2 solids content 15.2 wt %, primary particle size 5 nm, and pH value ∼1.0. The domain crystal structure of TiO_2 is anatase. The nearly transparent sol is long-term stabilized by a mineral acid (nitric acid). The UV/vis absorbance spectrum of the TiO_2 slurry is also shown in Figure 2. As is shown by Figure 2, the existence of TiO_2 slurry almost does not interfere with the methylene blue analysis by UV/vis spectrophotometer. Another commercial dye, HF6 coral pink with the main ingredient of triphenylmethane (Taipei First Chemical Company, Taiwan), was used for the same reaction to test the rate equation for its generalization.

Apparatus. The jacketed photocatalytic reactor system schematically shown in Figure 3 is made of Pyrex glass. A magnetic stirrer (Mirak S72725, Barnstead Thermolyne, U.S.A.) was used to control the agitation speed. The germicidal lamp (model FL4BLB, 4W, Sankyo, Japan) with the maximum light intensity at 365 nm was used as the light source. A temperature controller (water bath D-630, Deng Yng, Taiwan) was used to control the reaction temperature at desired levels. A pH apparatus (PC-310, Suntex, Taiwan) was used to measure the solution pH during reaction. A pump (Masterflex L/S digital standard drive, model 7518-00, Cole-Parmer, U.S.A.) was used to recirculate the reaction solution through a flow cell of the UV/vis spectrophotometer (Jasco V-560, Japan) to measure the concentration of methylene blue continuously. A dissolved oxygen pocket meter (Oxi 330i, WTW, Germany) with an

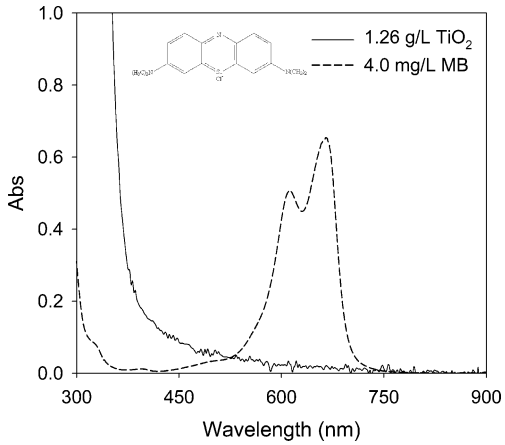

Figure 2. UV/vis absorbance spectrum of methylene blue solution and TiO_2 suspension.

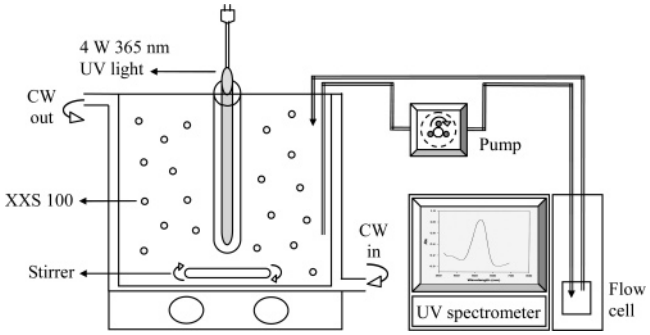

Figure 3. Schematic diagram of the smaller photocatalytic reactor system.

oxygen sensor (CellOx 325, WTW, Germany) was used to measure the initial solution dissolved oxygen concentration. To study the effect of UV light intensity on methylene blue reaction rate, another large photocatalytic reactor system was used. Figure 4 schematically shows the large jacketed photocatalytic reactor system (Jyi Goang, Taiwan) with the reactor made of stainless steel and equipped with a 20 W dc motor to control the agitation speed at the desired levels. In the large reactor system, 12 sets of 365 nm, 8 W UV lamps (model FL8BLB, 8W, Sankyo, Japan) were used to allow independent control of the on/off status of each UV lamp.

Procedures. In each test run, deionized water (1.5 L) was charged to the photocatalytic reactor and the agitating and temperature control system were turned on. The desired amount of XXS 100 TiO_2 sol was added to the reactor and uniformly mixed with the deionized water for 5 min, and then the UV/vis absorbance at 665 nm was read as the reference. The methylene blue solution with the desired initial concentration was added to the photocatalytic reactor and uniformly mixed with the TiO_2 solution for 15 min, and then another UV/vis absorbance at 665 nm was read as the reference. During this period, only a few methylene blue molecules were absorbed onto the TiO_2 surface without reaching equilibration. This procedure was discussed in the reaction mechanism part. Upon adding the methylene blue solution, the pH monitoring system was started to monitor the solution pH during reaction. Because the TiO_2 sol is long-term stabilized by the nitric acid and its pH value is ∼1.0, after being added into 1.5 L of deionized water, the solution pH is almost equal to 3.0. To discuss the effect of solution pH, nitric acid and NaOH were added to adjust solution pH before starting the reaction. The UV light was then turned on, and the concentration of the methylene blue was continuously measured

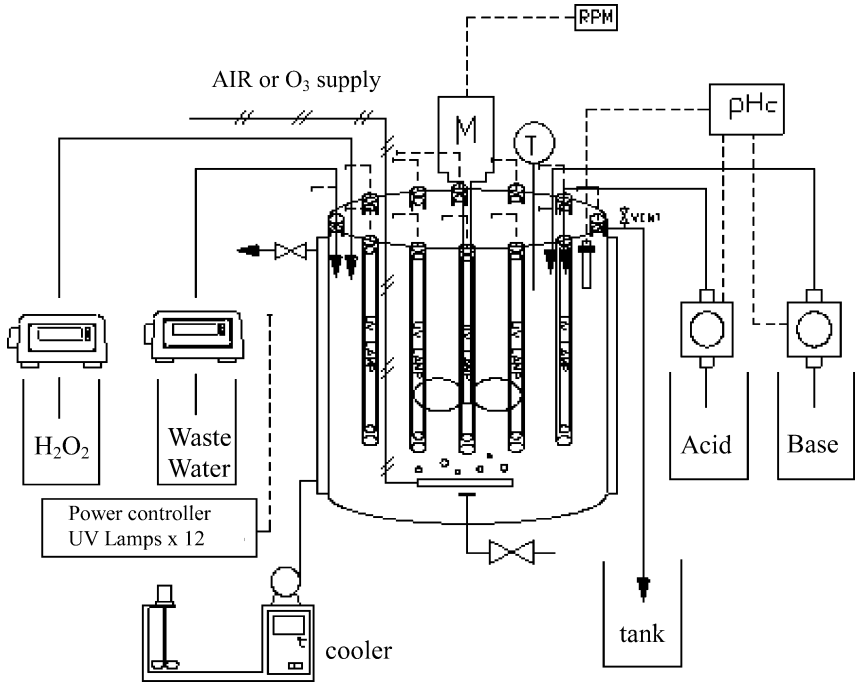

Figure 4. Schematic diagram of the larger photocatalytic reactor system.

Table 1. Operating Conditions of All Experimental Test Runs

operation parameters	range
agitating speed	100−600 rpm
recirculation flow rate	20−100 mL/min
DO concentration	2.07−28.4 mg/L
MB concentration	1.23−8.58 mg/L
reaction temperature	15−45 °C
TiO_2 dosage	0.09−1.26 g/L
UV light intensity	0−132 μW/cm^2

by the UV/vis spectrophotometer at $\lambda_{max} = 665$ nm with a calibration curve fitted by the Beer−Lambert's law. As is shown in Figure 2, the absorbance of TiO_2 suspension solution occurs at a wavelength <400 nm; hence, the existence of TiO_2 almost does not interfere with the methylene blue concentration measurement. The experimental procedure used to study the UV light effect in the larger reactor system is the same as that used in the smaller system except that 15 L of deionized water was added to the reactor initially. The operating conditions of all the experimental test runs are summarized in Table 1.

Results and Discussion

Effect of Solution pH. The solution pH is a very important operation parameter of photocatalytic reaction. Hoffmann et al.[28] reviewed a lot of studies and concluded that the interaction of TiO_2 with cationic electron donors and electron acceptors would be favored for heterogeneous photocatalytic activity at high pH greater than the zero point charge of TiO_2 (~4.5), while anionic electron donors and electron acceptors would be favored at low pH less than the zero point charge of TiO_2. Therefore, a suitable solution pH is needed for photocatalytic reactions. Our preliminary experiments show that, when the solution pH is <4.0, the nanophotocatalysts are well-dispersed in the solution and the suspension appears transparent or semitransparent. The solution pH has no noticeable effect on the methylene blue reaction rate for a solution pH <4.0. However, when the solution pH is >4.68, the TiO_2 particles rapidly coagulate and form visible sediments on the bottom. This coagulation and sedimentation process markedly reduces the TiO_2 surface area so that the decomposition rate of methylene blue significantly decreases. For the above reasons, we keep the solution pH <3 for all the test runs. In our experimental results, the methylene blue residual fraction exponentially decreases with the reaction time but the solution pH almost remained constant.

Effects of Agitation Speed and Recirculation Flow Rate. The next series of experimental tests performed in this study was to vary the agitation speed while keeping all other factors constant. From our previous experimental results, the methylene blue reaction rate increases with increasing agitation speed up to 300 rpm; for the agitation speed >300 rpm, the reaction rate remains unaffected by the agitation speed. We therefore use 300 rpm for all the other test runs. In our reactor system, we use a pump to recirculate the methylene blue solution to a UV/vis spectrophotometer. According to our data, the methylene blue reaction rate does not change significantly at varying recirculation rate. We therefore use 60 mL/min for all the other test runs. Using this recirculation flow rate and the total volume of the tubing, the time delay between the photocatalytic reactor and the UV flow cell is calculated to be <1 s. In our reaction system, the methylene blue concentration does not change significantly during this small time period so that we neglect the time-delay effect in our system.

For any chemical reactions influenced by mass transfer, the overall rate resistance is the summation of the mass-transfer resistance and the chemical reaction resistance. To study the intrinsic methylene blue decomposition kinetics, we use 300-rpm agitation speed and 60-mL/min recirculation flow rates for the test runs. In our reactor system, the agitation speed and recirculation flow rate are high enough so that the mass-transfer resistance does not affect the overall kinetics.

Effect of Initial DO Concentration. Dissolved oxygen (DO) is a good electron acceptor to receive electron transfer from excited TiO_2 valance band. Therefore, the next series of experiments was to vary the initial DO concentration by pure nitrogen purge or oxygen aeration but to keep other operation parameters constant. However, our experimental results show

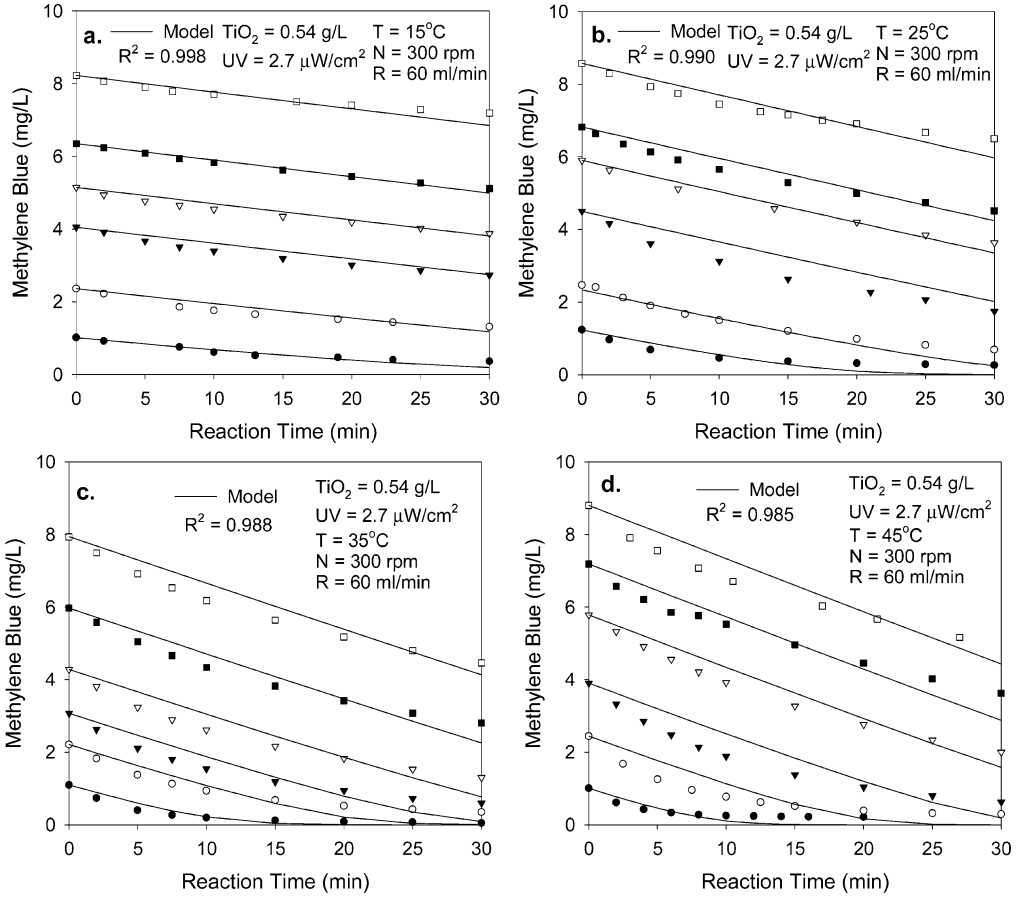

Figure 5. Experimental and predicted methylene blue concentration histories at varying initial methylene concentrations.

that the initial dissolved oxygen concentration does not affect the reaction rate. This suggests that the rate contribution from the superoxide radical pathway is much smaller than that from the hydroxyl radical pathway, i.e., $k'_{23}[O_2] \ll k_{23}$. All the terms associated with k'_{23} in eq 11 can be eliminated; therefore, eq 11 becomes

$$-r_{\text{dye}} = k_{01}k_{12}k_{23}[h\nu][\text{dye}][\text{TiO}_2]/ \\ k_{10}(k_{21}+k_{23}) + k_{12}k_{23}[h\nu] + k_{01}(k_{21}+k_{23})[\text{dye}] + \\ \left(1+\frac{k_{23}}{k_{34}}\right)k_{01}k_{12}[\text{dye}][h\nu] \quad (12)$$

After regrouping and lumping the coefficients, eq 12 can be rearranged as

$$-r_{\text{dye}} = \frac{k_4[h\nu][\text{dye}][\text{TiO}_2]}{1 + k_1[h\nu] + k_2[\text{dye}] + k_3[\text{dye}][h\nu]} \quad (13)$$

where the kinetics parameters k_1-k_4 are lumped coefficients that can be expressed in terms of the rate coefficients of the reaction steps.

$$k_1 = \frac{k_{12}k_{23}}{k_{10}(k_{21}+k_{23})}; \quad k_2 = \frac{k_{01}}{k_{10}};$$

$$k_3 = \frac{k_{01}k_{12}(k_{23}+k_{34})}{k_{10}k_{34}(k_{21}+k_{23})}; \quad k_4 = \frac{k_{01}k_{12}k_{23}}{k_{10}(k_{21}+k_{23})} \quad (14)$$

Effect of Initial Methylene Blue Concentration. After obtaining the rate equation, we carried out another series of experiments in which the initial methylene blue concentration was varied from 1.23 to 8.58 mg/L. The experimental results at varying initial methylene blue concentrations at 25 °C are shown in Figure 5b. In this series of experiments, the UV light intensity and TiO_2 dosage are kept constant; thus, eq 13 can be divided by $1 + k_1[h\nu]$ and becomes

$$-r_{\text{dye}} = \frac{k'_a[\text{dye}]}{1 + k'_b[\text{dye}]} \quad (15)$$

where k'_a and k'_b are lumped parameters that can be expressed in terms of the UV light intensity, the TiO_2 concentration, and the other kinetic parameters.

$$k'_a = \frac{k_4[h\nu][\text{TiO}_2]}{1 + k_1[h\nu]} \; k'_b = \frac{k_2 + k_3[h\nu]}{1 + k_1[h\nu]} \quad (16)$$

Equation 15 is similar to the Langmuir−Hinshelwood rate law. Since the initial rate method is less accurate than the integrating method, we use the integrated equation to obtain more precise kinetic parameters. Equation 15 can be integrated to obtain the transient methylene blue concentration,

$$\int_{C_0}^{C_t} \frac{1 + k'_b[\text{dye}]}{[\text{dye}]} d[\text{dye}] = \int_0^t -k'_a \, dt \quad (17)$$

or

$$\ln\left(\frac{C_t}{C_0}\right) + k'_b(C_t - C_0) = -k'_a t \quad (18)$$

To obtain the kinetic parameters k'_a and k'_b, the nonlinear regression method in the IMSL subroutine of Compaq Visual

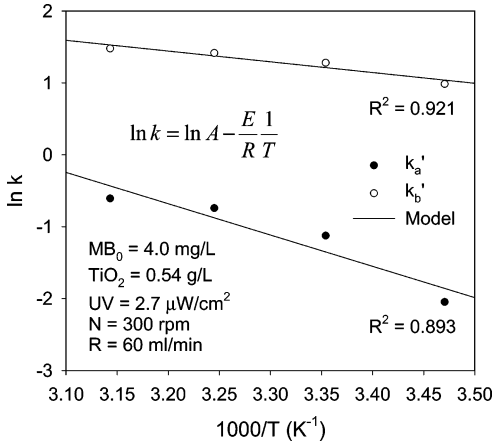

Figure 6. Effect of reaction temperature on the kinetic parameters.

Table 2. Model Parameters to Fit the MB Transient Concentration versus Initial MB Concentration at Varying Temperatures

parameter	15 °C	25 °C	35 °C	45 °C	units
k'_a	0.129	0.325	0.477	0.546	min^{-1}
k'_b	2.677	3.592	4.116	4.381	L/mg

Table 3. Temperature Correlation Parameters for Equation 15

parameter	for k'_a	for k'_b
A	5.77×10^5 min^{-1}	5.03×10^2 L/mg
E	36.23 kJ/mol	12.41 kJ/mol

Fortran was used. The parameters k'_a and k'_b for the test runs with varying initial MB concentrations at 25 °C are listed in Table 2. Figure 5b shows the experimental concentration histories and the transient concentrations predicted by the kinetic model using the same set of parameters k'_a and k'_b at 25 °C. As is shown by Figure 5b, eq 18 fits the experiment data satisfactorily. Although a similar Langmuir−Hinshelwood rate form is also commonly used in the literature, eq 15 is derived from the reaction mechanism without assuming which step is the rate-determining step or the equilibrium step. Therefore, eq 15 is a more general rate equation for MB decomposition kinetics and can be used for reactor design and scale-up with more confidence.

Effect of Reaction Temperature. After confirming the reaction kinetic model at 25 °C, another series of experiments was performed at varying reaction temperatures from 15 to 45 °C. Because dye wastewaters are usually at higher temperatures than other wastewater effluents, we cover the reaction temperature up to 45 °C. Figure 5 shows the experimental and predicted (by eq 18) transient MB concentration curves at varying temperatures. As is shown by Figure 5, eq 18 satisfactorily fits the transient concentrations at all the reaction temperatures using the parameters k'_a and k'_b listed in Table 2. One can see from Table 2 that both kinetic parameters k'_a and k'_b increase with the reaction temperature. It should be noted that k'_a and k'_b are not simple rate coefficients; they are lumped kinetic parameters as shown by eq 16. Trying to correlate these lumped kinetic parameters with temperature is very difficult because the activation energy of each individual step is unknown. However, Figure 6 shows that the kinetic parameters k'_a and k'_b listed in Table 2 can be roughly correlated with the reaction temperature by the Arrhenius law $k = A\ e^{-E/RT}$ with the parameters A and E listed in Table 3. The E value, 36 kJ/mol, for k'_a can be viewed as the apparent activation energy of MB decomposition reaction, while the E value, 12 kJ/mol, for k'_b probably represents the apparent activation energy of MB adsorption onto the photocatalyst. The apparent activation energy of MB

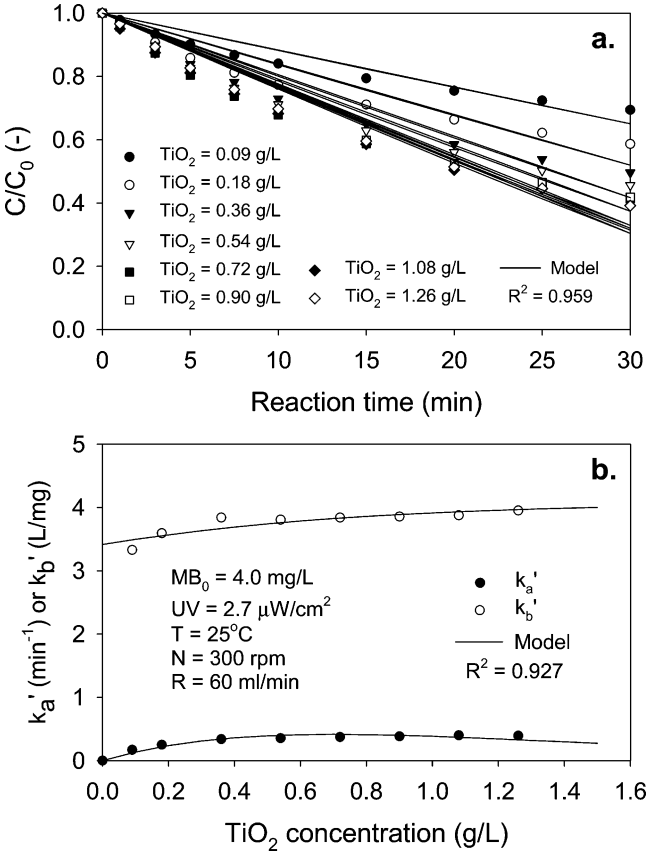

Figure 7. Effect of TiO_2 concentration on methylene blue decomposition kinetics.

decomposition obtained in this study is higher than those found in other studies. For example, Ling et al.[13] stated that the photocatalytic oxidation process did not require heating because it is initiated by photonic activation itself, so that the activation energy was very small and ranged from 5 to 20 kJ/mol.[29] This range of activation energy was very close to that of a hydroxyl radical reaction and suggested that organic compound decomposition by photocatalytic reaction might be controlled by the hydroxyl radical reaction. It is important to note that the lumped parameters, k'_a and k'_b, are combinations of different reaction coefficients and adsorption/desorption rate coefficients. The effect of temperature on these two parameters is more complicated than that on the rate coefficient of a single-step reaction. In general, the activation energy of a physical process such as adsorption is lower than that of a chemical process such as reaction. Therefore, the data in Table 2 shows that change of k'_a with the reaction temperature is more significant than that of k'_b.

Effect of TiO_2 Concentration. A series of MB decomposition tests were carried out with TiO_2 solid content being varied from 0.09 to 1.26 g/L, and the results are shown in Figure 7a. As is shown in Figure 7a, the methylene blue decomposition rate seems to increase with increasing TiO_2 concentration up to a certain value and then slightly decreases with increasing TiO_2 concentration. This result is contradictory with eq 13, which predicts that the decomposition rate is proportional to the TiO_2 concentration. However, this fact can be explained by the availability of active sites on the TiO_2 surface and the photoactivating light penetration in the suspension. The availability of the active sites increases with the catalyst concentration in the suspension, but the light penetration decreases with the catalyst concentration in the suspension due to the screening effect.[30]

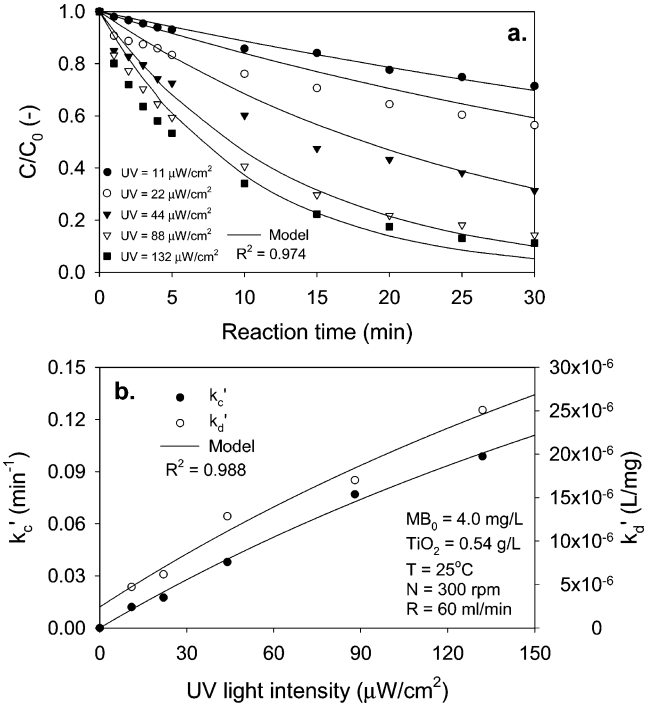

Figure 8. Effect of UV light intensity on methylene blue decomposition kinetics.

Equation 18 is also used to fit the experimental data shown in Figure 7a, and the obtained kinetics parameters k'_a and k'_b are shown in Figure 7b. As is shown in Figure 7b, the obtained k'_a is not proportional to the TiO_2 concentration and the obtained k'_b is not independent of the TiO_2 concentration as shown by eq 16. Although the existence of TiO_2 suspension almost does not interfere with the MB concentration measurement by UV/vis, the TiO_2 suspension absorbs UV/vis at 365 nm as shown by Figure 2. This suggests the 365 nm UV light intensity will be affected by the TiO_2 concentration. To account for this TiO_2 screening effect, we use a first-order correlation for the effective UV energy received by the TiO_2 particles:

$$[h\nu] = I_0\, e^{-k_5[TiO_2]} \tag{19}$$

Combining eq 16 and eq 19 leads to

$$k'_a = \frac{k_4 I_0\, e^{-k_5[TiO_2]}\cdot[TiO_2]}{1 + k_1 I_0\, e^{-k_5[TiO_2]}};\quad k'_b = \frac{k_2 + k_3 I_0\, e^{-k_5[TiO_2]}}{1 + k_1 I_0\, e^{-k_5[TiO_2]}} \tag{20}$$

The nonlinear regression tools in software Sigmaplot (SPSS Inc., Ver. 8.0) was used to obtain the parameters k_1-k_5, and the predicted k'_a and k'_b by eq 20 were also shown in Figure 7b with the parameters shown in eq 21.

$$k'_a = \frac{0.458 I_0\, e^{-1.523[TiO_2]}\cdot[TiO_2]}{1 + 0.049 I_0\, e^{-1.523[TiO_2]}}$$

$$k'_b = \frac{4.081 + (2.64\times10^{-8}) I_0\, e^{-1.523[TiO_2]}}{1 + 0.049 I_0\, e^{-1.523[TiO_2]}} \tag{21}$$

As shown in Figure 7, the kinetic model, eq 13, along with the TiO_2 screening model, eq 19, fit the MB decomposition kinetics at varying TiO_2 concentrations satisfactorily and also prove that the revised reaction mechanism is more suitable to explain the screening effect.

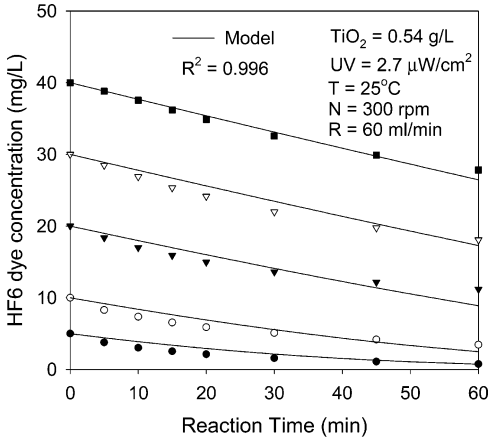

Figure 9. Experimental and predicted HF6 dye concentration histories at varying initial dye concentrations.

Effect of UV Light Intensity. Because the UV light irradiation on the TiO_2 surface will affect the hydroxyl radical generation, the last series of experiments was to vary the UV light intensity from 11 to 132 $\mu W/cm^2$. The experimental and predicted results at varying UV light intensity are shown in Figure 8a. Although not shown in Figure 8a, we found that methylene blue did not decompose at all without the UV irradiation. In this series of experiments, TiO_2 dosage is a constant so that the parameters k'_a and k'_b in eq 20 can be replaced by parameters k'_c and k'_d, respectively, using different parameters k_6-k_9 as shown in eq 22.

$$k'_c = \frac{k_9 I_0}{1 + k_6 I_0}$$

$$k'_d = \frac{k_7 + k_8 I_0}{1 + k_6 I_0} \tag{22}$$

Again, we used the nonlinear regression tool to obtain the parameters, k_6-k_9, and the predicted results by eq 23 are also shown in Figure 8b.

$$k'_c = \frac{(9.89\times10^{-4}) I_0}{1 + (2.25\times10^{-3}) I_0}$$

$$k'_d = \frac{2.41\times10^{-6} + (2.23\times10^{-7}) I_0}{1 + (2.25\times10^{-3}) I_0} \tag{23}$$

As shown in parts a and b of Figure 8, the effect of UV light intensity on the MB decomposition kinetics can be satisfactorily predicted by the model developed in this study. The effect of UV light intensity on the MB decomposition rate is comparable with the results of other studies. For example, Ollis et al.[31] stated that, at low light intensities, the reaction rate would increase linearly with increasing light intensity (first order), at intermediate light intensities beyond a certain value, the reaction rate would depend on the square root of the light intensity (half order), and at high light intensities, the reaction rate was independent of the light intensity. According to eq 13, the reaction rate is between zeroth and first order. Therefore, we expect eq 13 can be used in the general case to correlate the dye decomposition rate with the dye concentration, the photocatalyst concentration, and the UV light intensity I_0.

Model Testing. To test if the rate equation developed in this study is also applicable to other dye decomposition system, a commercial peach red dye HF6, for which the wavelength at

the maximum absorbance is 524 nm, was used to perform another series of experiments. The experimental procedure is the same, and the dye concentration histories at varying initial dye concentrations are shown in Figure 9. Equation 18 was also used to fit the experimental curves, and the obtained kinetics parameters k'_a and k'_b are 0.044 min^{-1} and 0.163 mg^{-1} L, respectively. The agreement of the predicted and experimental dye concentration curves shown in Figure 9 suggests that the general rate equation developed in this study is also applicable to other dye compounds. Because the general rate equation, eq 13, is obtained from considering the reaction mechanism and no rate-determining step is assumed, we expect it can be applied for the kinetics of photodecomposition of other organic compounds.

Conclusions

The methylene blue decomposition kinetics by nanosize TiO_2 suspension was experimentally studied by varying the agitation speed, the recirculation flow rate, the dissolved oxygen concentration, the TiO_2 dosage, the initial methylene blue concentration, the reaction temperature, and the UV light intensity. A general rate equation has been developed from considering the reaction mechanism by literature survey and our experimental conditions. This rate equation is obtained from using a systematic reaction network reduction technique to avoid the need of more restrictive assumptions commonly used, such as a rate-determining step or equilibrium steps. The resulting rate equation is able to predict the effects of initial MB concentration, temperature, TiO_2 concentration, and UV light intensity. The developed rate equation is also applicable to other dye compounds and is expected to be applicable to the decomposition kinetics of other organic compounds.

Literature Cited

(1) Malik, P. K. Dye removal from wastewater using activated carbon developed from sawdust: Adsorption equilibrium and kinetics. *J. Hazard. Mater.* **2004**, *113*, 81.

(2) Koyuncu, I. Reactive dye removal in dye/salt mixtures by nanofiltration membranes containing vinylsulphone dyes: Effects of feed concentration and cross-flow velocity. *Desalination* **2002**, *143*, 243.

(3) El-Daly, H. A.; Habib, A. F. M.; El-Din, M. A. B. Kinetics and mechanism of the oxidative color removal from Durazol Blue 8 G with hydrogen peroxide. *Dyes Pigm.* **2003**, *57*, 197.

(4) Ogutveren, U. B.; Gonen, N.; Koparal, S. Removal of dyestuffs from wastewater: Electrocoagulation of acilan blau using soluble anode. *J. Environ. Sci. Health, Part A, Environ. Sci. Eng.* **1992**, *27*, 1237.

(5) Ge, J.; Qu, J. Ultrasonic irradiation enhanced degradation of azo dye on MnO_2. *Appl. Catal., B: Environ.* **2004**, *47*, 133.

(6) Chu, W. Dye removal from textile dye wastewater using recycled alum sludge. *Water Res.* **2001**, *35*, 3147.

(7) Tan, B. H.; Teng, T. T.; Omar, A. K. M. Removal of dyes and industrial dye wastes by magnesium chloride. *Water Res.* **2000**, *34*, 597.

(8) Ince, N. H.; Tezcanli, G. Treatability of textile dye-bath effluents by advanced oxidation: preparation for reuse. *Water Sci. Technol.* **1999**, *40*, 183.

(9) Sadik, W.; Shama, G. UV-induced decolourization of an azo dye by homogeneous advanced oxidation processes. *Process Saf. Environ. Prot. Trans. Inst. Chem. Eng., Part B* **2002**, *80*, 310.

(10) Arslan, I.; Balcioglu, I. A.; Tuhkanen, T. Treatability of simulated reactive dye-bath wastewater by photochemical and nonphotochemical advanced oxidation processes. *J. Environ. Sci. Health, Part A* **2000**, *35*, 775.

(11) Peller, J.; Vinodgopal, K. Hydroxyl radical-mediated advanced oxidation processes for textile dyes: A comparison of the radiolytic and sonolytic degradation of the monoazo dye Acid Orange 7. *Res. Chem. Intermed.* **2003**, *29*, 307.

(12) Kominami, H.; Kumamoto, H.; Kera, Y.; Ohtani, B. Photocatalytic decolorization and mineralization of malachite green in an aqueous suspension of titanium(IV) oxide nanoparticles under aerated conditions: Correlation between some physical properties and their photocatalytic activity. *J. Photochem. Photobiol. A* **2003**, *160*, 99.

(13) Ling, C. M.; Mohamed, A. R.; Bhatia, S. Performance of photocatalytic reactors using immobilized TiO2 film for the degradation of phenol and methylene blue dye present in water stream. *Chemosphere* **2004**, *57*, 547.

(14) Lakshmi, S.; Renganathan, R.; Fujita, S. Study on TiO_2-mediated photocatalytic degradation of methylene blue. *J. Photochem. Photobiol. A* **1995**, *88*, 163.

(15) Wang, Y. Solar photocatalytic degradation of eight commercial dyes in TiO_2 suspension. *Water Res.* **2000**, *34*, 990.

(16) Sakthivela, S.; Neppolianb, B.; Shankarb, M. V.; Arabindoob, B.; Palanichamyb, M.; Murugesan, V. Solar photocatalytic degradation of azo dye: comparison of photocatalytic efficiency of ZnO and TiO_2. *Sol. Energy Mater. Sol. Cells* **2003**, *77*, 65.

(17) Ollis, D. F. Contaminant degradation in water: Heterogeneous photocatalysis degrades halogenated hydrocarbon contaminants. *Environ. Sci. Technol.* **1985**, *19*, 480.

(18) Sivalingam, G.; Nagaveni, K.; Hegde, M. S.; Madras, G. Photocatalytic degradation of various dyes by combustion synthesized nano anatase TiO_2. *Appl. Catal., B: Environ.* **2003**, *45*, 23.

(19) Xu, N. P.; Shi, Z. F.; Fan, Y. Q.; Dong, J. H.; Shi, J.; Hu, Z. C. Effects of particle size of TiO_2 on photocatalytic degradation of methylene blue in aqueous suspensions. *Ind. Eng. Chem. Res.* **1999**, *38*, 373.

(20) Helfferich, F. G. Systematic Approach to Elucidation of Multistep Reaction Networks. *J. Phys. Chem.* **1989**, *93*, 6676.

(21) Chern, J.-M.; Helfferich, F. G. Effective Kinetic Modeling of Multistep Homogeneous Reactions. *AIChE J.* **1990**, *36*, 1200.

(22) Chern, J. M. General rate equation and their application for cyclic reaction networks: Single-cycle systems. *Ind. Eng. Chem. Res.* **2000**, *39*, 4100.

(23) Chen, T. S.; Chern, J. M. General rate equation and their application for cyclic reaction networks: Multi-pathway systems. *Chem. Eng. Sci.* **2002**, *57*, 5011.

(24) Helfferich, F. G. *Kinetics of multistep reactions*, 2nd ed.; Elsevier: Amsterdam, 2004.

(25) Fujishima, A.; Rao, T. N.; Tryk, D. A. Titanium dioxide photocatalysis. *J. Photochem. Photobiol. C* **2000**, *1*, 1.

(26) Galindo, C.; Jacques, P.; Kalt, A. Photodegradation of the aminoazobenzene acid orange 52 by three advanced oxidation processes: UV/H_2O_2, UV/TiO_2 and VIS/TiO_2: Comparative mechanistic and kinetic investigations. *J. Photochem. Photobiol. A* **2000**, *130*, 35.

(27) Habibi, M. H.; Hassanzadeh, A.; Mahdavi, S. The effect of operational parameters on the photocatalytic degradation of three textile azo dyes in aqueous TiO_2 suspensions. *J. Photochem. Photobiol. A* **2005**, *172*, 89.

(28) Hoffmann, M. R.; Martin, S. T.; Choi, W.; Bahnemann, D. W. Environmental application of semiconductor photocatalysis. *Chem. Rev.* **1995**, *95*, 69.

(29) Chen, D. W.; Sivakumar, M.; Ray, A. K. Heterogeneous photocatalysis in environmental remediation. *Dev. Chem. Eng. Miner. Process.* **2000**, *8*, 505.

(30) Konstantinou, I. K.; Albanis, T. A. TiO_2-assisted photocatalytic degradation of azo dyes in aqueous solution: Kinetic and mechanistic investigations: A review. *Appl. Catal., B: Environ.* **2004**, *49*, 1.

(31) Ollis, D. F.; Pelizzetti, E.; Serpone, N. Photocatalyzed destruction of water contaminants. *Environ. Sci. Technol.* **1991**, *25*, 1522.

Received for review March 7, 2006
Revised manuscript received July 13, 2006
Accepted July 14, 2006

IE0602759